Available online at www.sciencedirect.com
SCIENCE DIRECT
Lithos 89 (2006) 154–173
LITHOS
www.elsevier.com/locate/lithos

Exhumation *P–T* path of UHP eclogites in the Hong'an area, western Dabie Mountains, China

Jingbo Liu [a,*], Kai Ye [a], Min Sun [b]

[a] *State Key Laboratory of Lithosphere Tectonic Evolution, Institute of Geology and Geophysics, Chinese Academy of Sciences, Beijing, 100029, China*
[b] *Department of Earth Sciences, The University of Hong Kong, Pokfulam Rd., Hong Kong*

Received 19 July 2004; accepted 11 December 2005
Available online 30 January 2006

Abstract

Four generations of mineral assemblages have been identified in ultrahigh-pressure (UHP) eclogites from the Hong'an area, recording four metamorphic stages of the exhumation trajectory, i.e., garnet + omphacite + kyanite + zoisite/epidote + rutile + coesite formed at the UHP stage, garnet + omphacite + paragonite + phengite + amphibole + epidote + quartz at the high-pressure (HP) eclogitic stage, amphibole + epidote + albite–oligoclase + paragonite + quartz at the epidote-amphibolite facies (EA) stage, and actinolite+ albite and pumpellyite + albite + K-feldspar + muscovite + chlorite + margarite + epidote + quartz at the greenschist facies (GS) stage. Garnet formed at the UHP stage was overgrown by atoll garnet at the HP stage. X-ray images, mineral compositions and compositional profiles indicate that the UHP garnet experienced a variable Fe–Mg modification in response to Fe–Mg exchange between garnet and omphacite prior to the overgrowth of atoll HP garnet. A volume diffusion zone was also observed between the UHP and HP garnets. The following *P–T* conditions were estimated for these mineral assemblages: 480 to 560 °C and 2.5 to 2.9 GPa with median values of 520 °C and 2.8 GPa at UHP stage, 575 to 685 °C and 1.6 to 1.9 GPa with the average results of 634 ± 37 °C and 1.8 ± 0.06 GPa at the HP stage, 500 to 640 °C and 0.4 to 1 GPa at the EA stage, and 160 to 320 °C and 0.2 to 0.8 GPa at the GS stage. The Hong'an UHP eclogites experienced a temperature increase of over 100 °C from the UHP to HP stages and continued to exhume from the HP to EA stages through a process of approximately isothermal depression, which was followed by a significantly cooling from the EA to GS stages. In the process of exhumation, UHP eclogites witnessed a series of events involving fluid influx, resulting in the formation of hydrous minerals at different stages. The nature of fluids changed from K-rich at the HP stage to K-poor at the EA stage and then K-rich again at the GS stage.

Keywords: UHP metamorphism; Eclogite; Coesite; *P–T* path; Exhumation; The Dabie Mountains

1. Introduction

Coesite- and diamond-bearing UHP metamorphic rocks are formed at great depths of over 90–150 km. The processes that form UHP metamorphic rocks and that allow their exhumation have become the subject of great interest. The UHP rocks in the Dabie–Sulu region of China are commonly partially overprinted by mineral assemblages developed at granulite (GR) or epidote-amphibolite, and greenschist grades during their exhumation process. On the basis of the *P–T* estimates provided by these retrograde assemblages, we can

* Corresponding author. Tel.: +86 10 62007822; fax: +86 10 62010846.
E-mail address: jingboliu@mail.igcas.ac.cn (J. Liu).

0024-4937/$ - see front matter © 2005 Elsevier B.V. All rights reserved.
doi:10.1016/j.lithos.2005.12.002

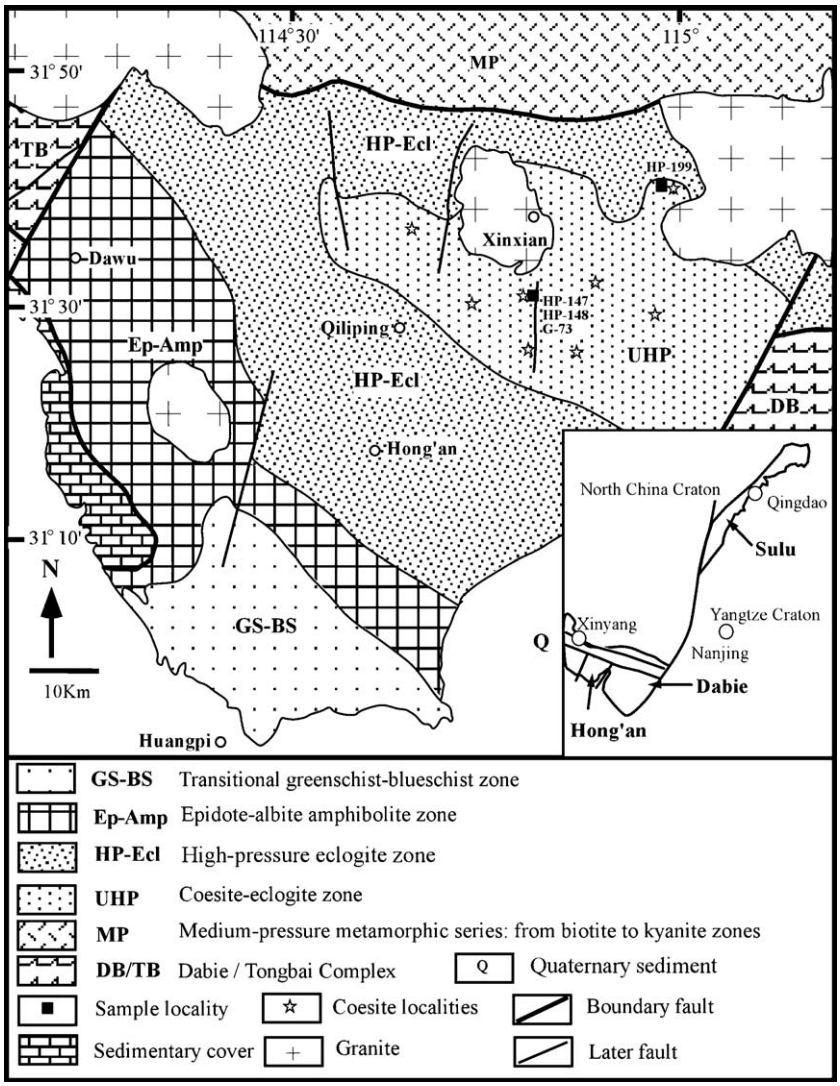

Fig. 1. Geological sketch map showing the metamorphic zones and sample localities in the Hong'an area.

construct a *P–T* path for the exhumation of these UHP rocks (Wang et al., 1992; Wang et al., 1993; Okay, 1993, 1995; Zhang and Liou, 1994, 1995a,b; Banno et al., 2000; Carswell and Zhang, 2000; Nakamura and Hirajima, 2000; Yao et al., 2000). The previously inferred *P–T* paths were constructed based on an underlying assumption that the UHP rocks reached their maximum temperatures and pressures synchronously, which led to the conclusion that their exhumation was accomplished by either isothermal or decreasing temperature uplift. The main problem for these inferred *P–T* paths is that re-equilibrium of the early UHP mineral assemblage during the subsequent process of exhumation was ignored. In fact, late retrograde metamorphic events possibly exert a great influence on the survival preserved compositions of early mineral assemblages as a result of volume diffusion of elements, recrystallization of minerals and metamorphic reactions that may result from the changing *P–T* conditions and the introduction of fluids. Therefore, in order to fully understand these UHP rocks we need to determine the degree of compositional modification of the UHP assemblage during exhumation, and to reconstruct the original UHP mineral compositions.

If the metamorphic temperature is relatively high, the compositions of minerals formed in the early stage will possibly be significantly modified during the subsequent metamorphic process to equilibrate with the new metamorphic conditions, which will probably hamper the reconstruction of original mineral compositions. The rocks in a UHP metamorphic zone that experienced relatively lower metamorphic temperatures possibly

preserve the mineral assemblages with original compositions due to relatively slow diffusion and reaction rates, and therefore they should be good candidates for reconstructing reliable exhumation *P–T* paths. The Hong'an area, western Dabie Mountains of China, is such a place that contains UHP eclogites with maximum temperatures lower than 700 °C (Zhang and Liou, 1994; Liu et al., 2004). The minerals of eclogites in the area, such as garnet, display striking compositional zoning (Liu et al., 2004). In this paper, we used X-ray compositional mapping to carefully study the UHP eclogites that contain atoll garnets, and to identify multi-stage mineral assemblages. The results have enabled us to build a more precise and reliable uplift trajectory of these UHP rocks. In addition, the hydrous minerals formed at different stages help us to unravel the nature of fluids in the process of exhumation.

2. Regional geology

The Qinling–Dabie–Sulu orogen resulted from the collision between the Yangtze and North China cratons in the Triassic (Ames et al., 1993; Li et al., 1993; Rowley et al., 1997; Hacker et al., 1998). The fault-bounded Hong'an area is the westernmost terrain in the orogen that preserves UHP eclogites (Fig. 1). It consists of a succession of metamorphic zones characterized by increasing metamorphic grade from transitional blueschist–greenschist, through epidote-amphibolite, high-pressure eclogite to coesite-bearing eclogite (Zhou et al., 1993; Zhang and Liou, 1994; Cui and Wang, 1995; Liu et al., 1996, 1998; Hacker et al., 1998; Eide and Liou, 2000). The UHP zone consists of gneisses, schists, and pods of glaucophane–kyanite bearing eclogites (Zhang and Liou, 1994). Coesite, or quartz pseudomorphs after coesite have been identified as inclusions in omphacite and garnet in this zone. The country rocks include light-colored, phengite-bearing quartzofeldspathic gneiss and dark-colored biotite–chlorite–epidote–amphibole–garnet gneiss. Coesite inclusions have also been identified in zircons from the phengite-bearing quartzofeldspathic gneiss by laser-Raman Spectroscopy (our unpublished data).

Extensive isotope geochronological studies suggest that the UHP metamorphism occurred at 220 to 240 Ma in the Dabie–Sulu region (Ames et al., 1993; Li et al.,

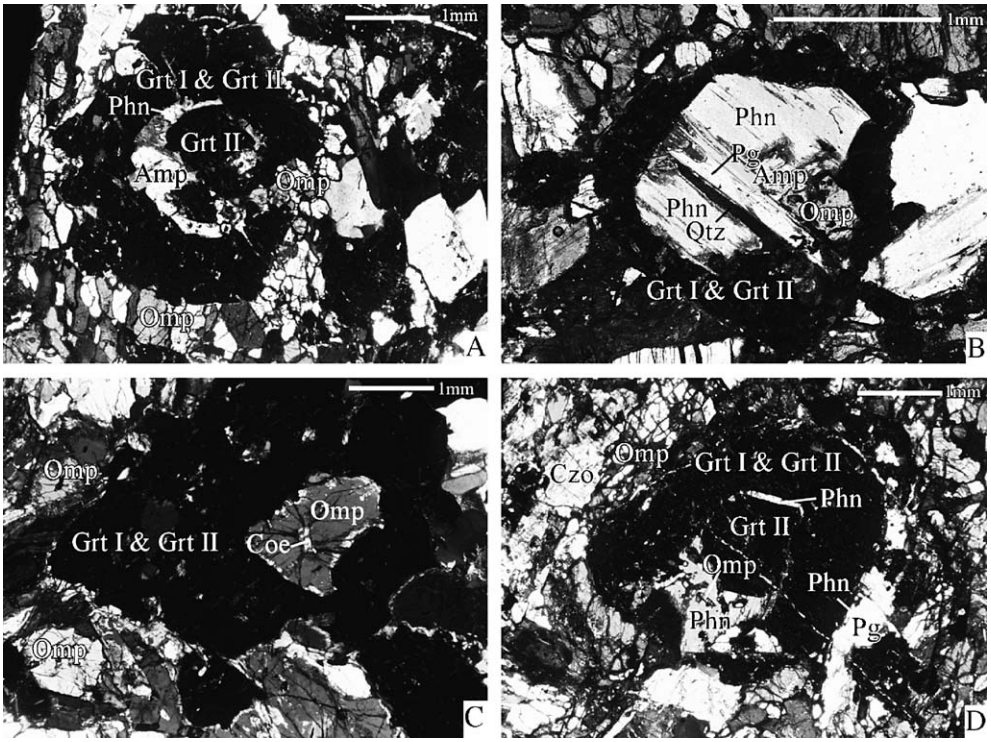

Fig. 2. Photomicrographs showing atoll garnets. (A) an atoll garnet (Grt I & Grt II) encloses amphibole (Amp), phengite (Phn), omphacite and garnet (Grt II) (G-73); (B) an atoll garnet (Grt I & Grt II) encloses amphibole, phengite and omphacite (G-73); (C) an atoll garnet (Grt I & Grt II) encloses a grain of omphacite that contains a inclusion of polycrystalline quartz after coesite (HP-147). The X-ray images of this garnet is shown in Fig. 3G–I; (D) an atoll garnet (Grt I & Grt II) encloses phengite, omphacite and Grt II (G-73). Mineral abbreviations are after Kretz (1983).

1993; Rowley et al., 1997; Hacker et al., 1998). Phengite cooling ages from blueschist through coesite-bearing eclogite facies rocks in the Hong'an area suggests that partial overprinting of the peak metamorphic assemblages occurred between 230 and 195 Ma (Eide et al., 1994). The short interval from the UHP to retrograde stages suggests that the lower grade overprints possibly occurred in the exhumation process, and the *P–T* path estimated for these rocks represents the *P–T* evolution in the exhumation process of the UHP rocks.

3. Description of samples

The eclogitic samples were collected within the UHP eclogite zone in the Hong'an area (Fig. 1). The eclogites occur as lenses or layers in the gneissic rocks. The eclogitic samples are characterized by atoll form of some grains of garnet (Fig. 2). On the basis of petrographic observation, the four generations of mineral parageneses were determined; these are made up of combinations of the minerals garnet, omphacite, kyanite, epidote, phengite, paragonite, amphibole, coesite, quartz, margarite, chlorite, pumpellyite and rutile, and formed at the UHP, HP, EA and GS stages, respectively (Table 1).

The UHP assemblage was identified on the basis of the occurrence of coesite and X-ray images of garnet. Atoll garnets are well developed in the samples (Fig. 2), and they enclose phengite, paragonite, epidote, amphibole, omphacite, and quartz. In the X-ray images of Mg and Ca, the atoll garnet consists of two parts, i.e., the early relict garnet (Grt I) with striking resorbed outline and the late overgrowth garnet (Grt II) (Fig. 3A, B, C, D and G, H, I). Garnets that lack an atoll structure are also composed of Grt I and Grt II (Fig. 3E, F and J, K, L). Grt I is characterized by low Mg and high Ca contents. It formed at the UHP stage, as evidenced by the occurrence of coesite inclusions (Fig. 3E and F), and its association with omphacite that contains coesite inclusions (Fig. 3G, H and I). The other inclusions in Grt I include epidote and zoisite. Kyanite is observed as a relict mineral in epidote of the EA stage (Fig. 3K), and is considered as a possible UHP phase. Therefore, we infer that the UHP assemblage consists of Grt I + omphacite + kyanite + coesite + epidote or zoisite.

Table 1
Mineral assemblages of the four stages

Stages	Mineral assemblages	Textures	Inferred fluids
UHP	Grt I + Omp + Ky + Ep/Czo + Coe		
HP	Grt II + Phn + Omp + Qtz + Ap	Atoll garnet	K-rich fluid
	Grt II + Phn + Ep + Qtz		
	Grt II + Phn + Amp + Om + Pg + Qtz		
	Grt II + Phn + Amp + Ep + Pg + Qtz		
	Grt II + Amp + Ep + Omp + Qtz + Pg	Non-atoll garnet Amp, Ep, Omp, Pg, Phn and Qtz occur as inclusions in Grt II	
	Grt II + Amp + Qtz + Pg		
	Grt II + Amp + Phn + Qtz + Ap		
EA	Amp + Ab–Olg	Symplectite Replacing Omp, Grt and Ky	K-poor fluid
	Amp + Ep + Pg + Qtz ± Ab–Olg		
GS	Act + Ab + Qtz	Symplectite Along fractures	K-rich fluid
	Pmp + Ms + Chl + Mrg + Ab + Kfs + Qtz		

Phn: phengite, Coe: coesite; Olg: oligoclase. Other mineral abbreviations are from Kretz (1983).

The HP assemblage is characterized by Grt II-related mineral growth. Grt II is more Mg-rich and Ca-poor than Grt I, and contains tiny inclusions of amphibole, paragonite and omphacite (Fig. 3E, I and J). Grt II replaced and overgrew Grt I together with a group of hydrous minerals such as phengite, paragonite, epidote and amphibole (Fig. 3). Different hydrous minerals occur in different domains of the sample (Table 1). Omphacite in the matrix coexists with Grt II. Phengite only occurs in domains where atoll garnet is developed, not in the matrix, and coexists with paragonite (Figs. 2B and 3A and C). This suggests that phengite formed at the HP stage rather than the UHP stage.

The EA stage developed three types of mineral assemblage: amphibole + epidote + quartz between garnet and omphacite, coarse-grained amphibole + epidote + paragonite + quartz ± albite–oligoclase in the matrix (Fig. 4A), and symplectites of albite–oligoclase + amphibole after omphacite. The coarse-grained assemblage grew at the expense of the early eclogitic mineral assemblage. Phengite has not been identified in the EA assemblages.

The mineral assemblages that define the GS stage developed along fractures. We have observed the assemblage of actinolite + albite in the fractures that pass through omphacite (Fig. 4). Along the same fractures, we have also observed the assemblage: pumpellyite + albite + K-feldspar + muscovite + chlorite + margarite + epidote + quartz (Fig. 4B).

4. Mineral analysis

Mineral compositions were analyzed using a Cameca SX-51 electron microprobe at the Institute of Geology and Geophysics, Chinese Academy of Sciences. An accelerating voltage of 15 kV, a beam current of 20 nA, and a beam diameter of 3 μm were set during the

analysis. For the analysis of omphacite, mica and plagioclase, a beam diameter of 8 μm was used. Natural and synthetic minerals were used for standard calibration. Representative analyses are reported in Table 2. The detection limits of a single spot are 75, 50, 52, 50, 100, 105, 125, 135, 175, 190, and 205 ppm for Na, Mg, Al, Si, K, Ca, Ti, Cr, Mn, Fe, and Ni, respectively. These were calculated by using the counting rate of the pure element, the background counting rate with 3σ and the counting time of the analyzed sample (Scott et al., 1995). Analytical errors (1σ) are 0.08, 0.05, 0.05, 0.04, 0.08, 0.08, 0.08, 0.12, 0.12, 0.12, and 0.12% for Na, Mg, Al, Si, K, Ca, Ti, Cr, Mn, Fe, and Ni, respectively. These were calculated by using the total peak counts, the total background counts, the peak counting time, and the background counting time of the analyzed sample (Scott et al., 1995). The X-ray compositional maps were obtained by stage scan at a resolution of 1024×1024 measured points and count time of 50 ms per point under operating conditions of 15 kV and 50 nA beam current.

4.1. Garnet

Grt I and Grt II have different compositional ranges (Fig. 5). However, the composition is transitional through the domain DZ marked in Fig 5. This transitional domain is shown both in X-ray images (Fig. 3A, G and J) and compositional profiles (Fig. 6). Grt I shows higher grossular and almandine contents, and lower pyrope contents than Grt II (Fig. 5, Table 2), which allows Grt I to be easily distinguished from Grt II in the X-ray compositional images (Fig. 3). Grt I has compositional variations in Fe^{2+} and Mg contents that show negative correlation at relatively constant Ca contents (Figs. 5 and 6). In some grains of Grt I, the Fe^{2+} and Mg contents are of very irregular zoning, as shown in X-ray compositional images (e.g., Fig. 3J, K and L). Some Mg-poor domains of homogenous composition (UD in Figs. 3, 5 and 6) occur as relict patches (e.g., Fig. 6 profiles 4 and 6) in Mg-rich domains of heterogeneous composition (CD in Figs. 3, 5 and 6). In other grains, Fe^{2+}, Mg and Ca are homogenously distributed except for the rim part of Grt I (Figs. 3E and F and 6 profile 3). These observations indicate that the compositional variations of Grt I are different in different garnet grains, and may be related to variably compositional modification after the formation of Grt I. In contrast, Grt II shows the following compositional variations (1) Fe^{2+} decreases and Mg increases at a relatively constant Ca content from the interior to the rim (Fig. 6. profiles 2 and 5), (2) Ca decreases and Mg increases from the interior to the rim at a relatively constant Fe content (Fig. 6 profile 3), and (3) $Ca+Fe^{2+}$ decreases and Mg increases from the interior to the rim (Fig. 6 profile 1). The concentric zoning of Grt II is manifested by regular compositional changes from the interior to the rim, and is clearly different from that of Grt I. In the outermost rim of some Grt II, we identified a zone of 5–25 μm width where Fe^{2+} significantly increases and Mg plummets (RZ in Fig. 6 profiles 1, 3 and 5).

4.2. Omphacite

Omphacite has a jadeite content from 42 to 59% (Fig. 7), and shows some compositional variations. The omphacites have been classified into the following three categories for a compositional comparison (Fig. 7): omphacite inclusions of >300 μm diameter in Grt I (Fig. 3E, G and J), in which coesite inclusions have been identified (Fig. 3G); omphacite inclusions of <50 μm diameter in Grt I; and omphacite in the matrix. Different omphacite types exhibit some compositional difference: the omphacite inclusions of >300 μm diameter have systematically higher Mg contents and lower Fe^{2+}/Mg ratio than the other two omphacite types. Omphacite in the matrix shows a large compositional range, and has systematically higher Na contents than the omphacite that occurs as inclusions (Fig. 7).

4.3. Amphibole

The chemical formula of amphibole is calculated in the form of $A_{0-1}B_2C_5T_8O_{22}(OH)_2$ (Leake et al., 1997). The maximum Fe^{3+} content was estimated by using the stoichiometric constraint of $T+C=13$, excluding Ca, Na and K at the T and C sites. The amphiboles that coexist with Grt II and the coarse-grained amphiboles in the EA stage are barroisite and taramite, whereas the amphibole in symplectite has the composition of hornblende, barroisite or taramite. Amphibole at the GS stage is actinolite (Table 2 and Fig. 8A).

4.4. White micas

Phengite, muscovite, and paragonite occur in the HP and GS assemblages. The Si content of phengite formed at the HP stage ranges from 3.45 to 3.66 cations per structural formula, and that of phengite and muscovite formed at the GS stage ranges from 3.10 to 3.30 (Fig. 8B). The high Si content of phengite indicates that the Grt II assemblage formed under high-pressure conditions. The ratio of $Na/(Na+K)$ for paragonite ranges from 0.89 to 0.96.

4.5. Feldspar

Plagioclase formed at both the EA and GS stages. It occurs as discrete grains of albite (Ab_{95-100}) and oliogoclase (Ab_{89-73}) at the EA stage, implying formation across the peristerite miscibility gap (Fig. 8C). At the GS stage, plagioclase formed as albite, and K-feldspar was formed as inclusions in muscovite (Fig. 4B).

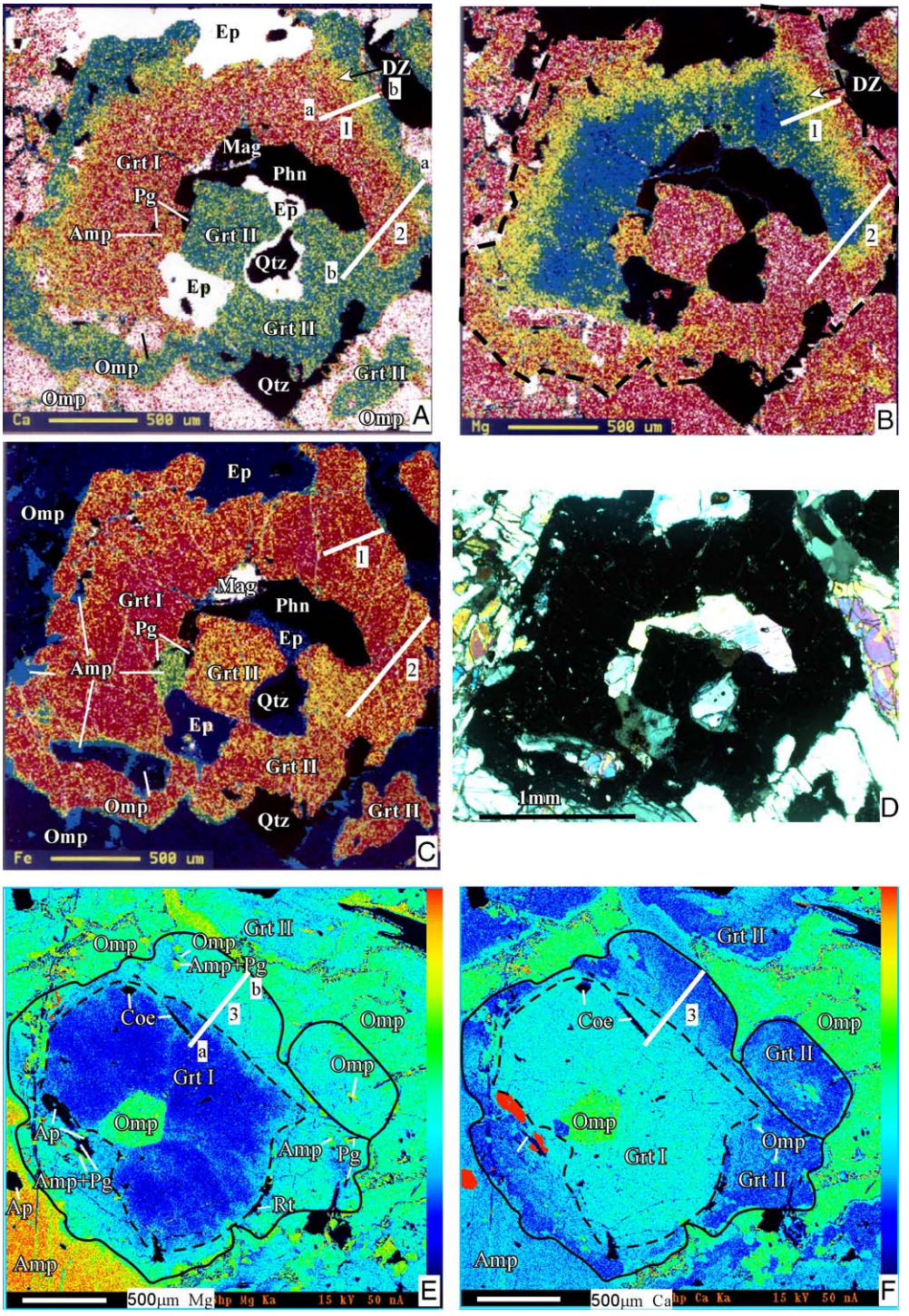

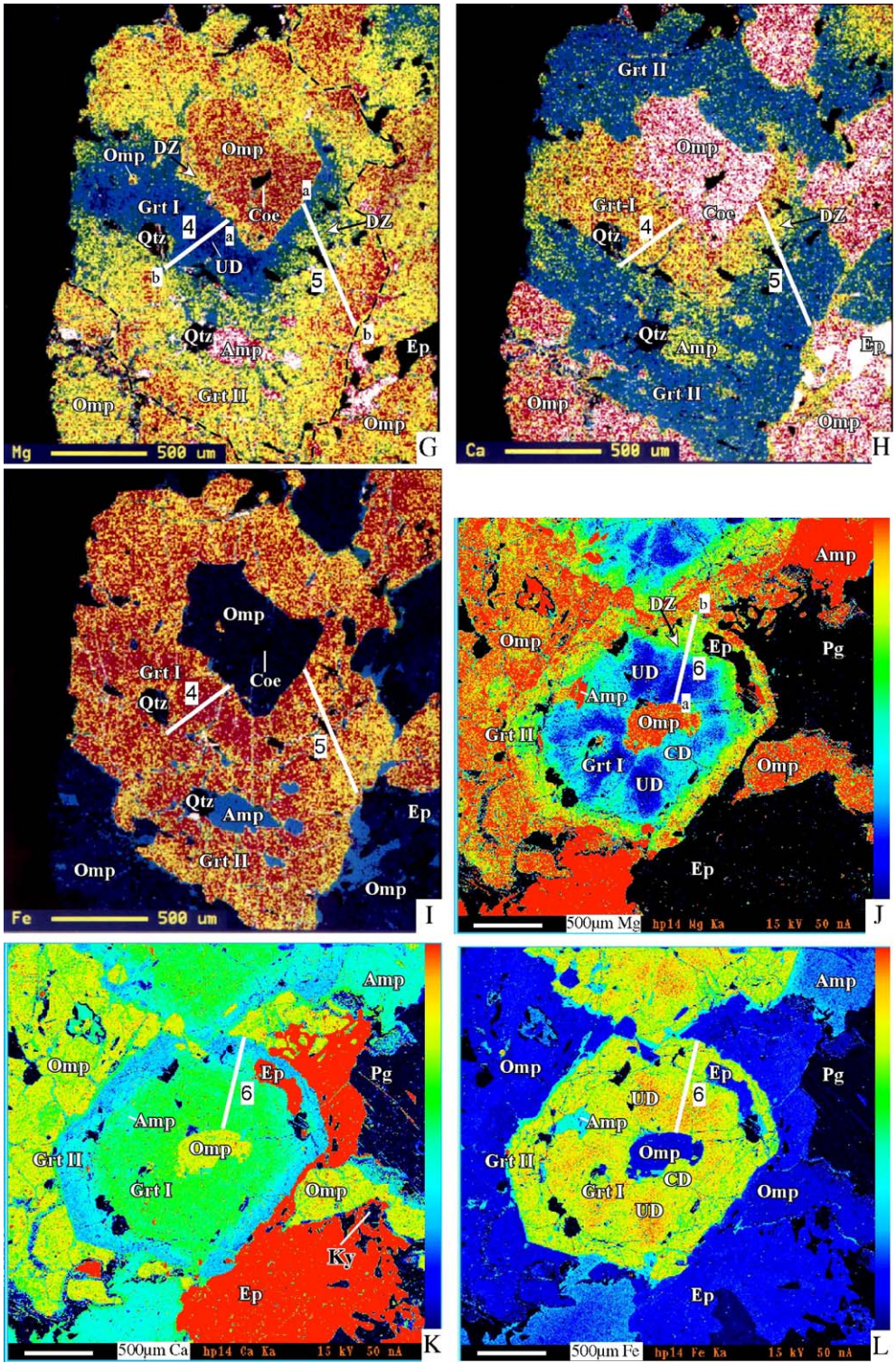
Omp
DZ
Grt I
Qtz
Coe
UD
Grt II
Amp
Ep
Pg
CD
Ky
Mg 500 um
Ca 500 um
Fe 500 um
500μm Mg hp14 Mg Ka 15 kV 50 nA
500μm Ca hp14 Ca Ka 15 kV 50 nA
500μm Fe hp14 Fe Ka 15 kV 50 nA
G
H
I
J
K
L

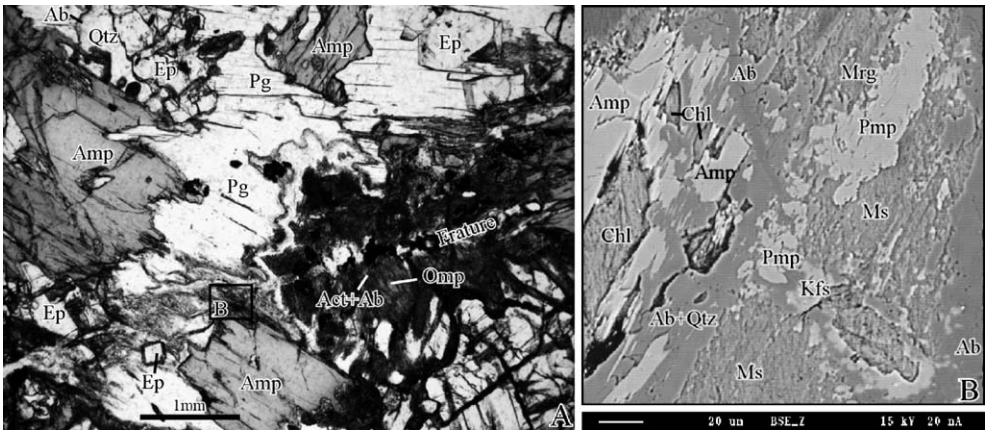

Fig. 4. Photomicrograph and back-scattered electron (BSE) image showing the mineral assemblages of the EA and GS stages. (A) photomicrograph showing the coarse-grained mineral assemblage of the EA stage (cross-polars) and the mineral assemblage of the GS stage along a fracture; (B) BSE image showing the pumpellite-bearing assemblage along the fracture (outlined by rectangle in A).

4.6. Epidote group minerals

Epidote group minerals formed at the UHP stage include discrete grains of zoisite (Ps 4%) and epidote (Ps 11–17%) (Fig. 8D), while those formed at the HP and EA stages are only epidote (Ps 9–19%, and 9–15%, respectively, Fig. 8D).

4.7. Other minerals

Chlorite, kyanite, margarite, magnetite, quartz, pumpellyite, rutile, sphene and zircon have been identified in the UHP rocks. Mineral compositions are presented in Table 2.

5. Discussion

5.1. Garnet zoning and omphacite evolution

As shown in Figs. 3, 5 and 6, garnet in the studied samples has been divided into Grt I, Grt II and a transitional compositional zone between Grt I and Grt II (DZ), and Grt I contains the UD and CD domains. The division is based on the interpretations on the X-ray compositional mapping (Fig. 3), pyrope–almandine–grossular triangle diagram (Fig. 5) and the compositional profiles (Fig. 6).

The pyrope content displays a negative correlation with almandine content in Grt I at the relatively constant grossular content, and this relationship results in the striking Fe and Mg zoning shown in X-ray compositional images (Fig. 3). The irregular patchy shape of the Fe-rich and Mg-poor domains in Grt I (e.g., Fig. 3J and L) suggests that these domains are relict parts of a UHP garnet that was mostly modified in its composition. The observations based on the compositional profiles (Fig. 6 profiles 3, 4 and 6) suggest that Grt I should be homogeneous at the very early stage, and that the Fe and Mg zoning was developed at a late process. This can be explained by variable substitution of Mg for Fe^{2+} in response to diffusion zoning that was produced by Fe^{2+}–Mg exchange. The substitution of Mg for Fe^{2+} in Grt I forms an evident trend towards Mg-rich directions shown in Fig. 5. The UD in Grt I is located at an end of this trend (Fig. 5), and therefore can be interpreted to be the domain that was not or less modified, and possibly preserves original compositions at UHP

Fig. 3. X-ray compositional images showing garnet zoning. (A–C) are the X-ray images of Ca, Mg and Fe (HP-147). (D) is a photomicrograph with cross-polars. The atoll garnet consists of an early relict garnet (Grt I) and a late-overgrowth garnet (Grt II). There is a transitional compositional zone (DZ) between Grt I and Grt II. Numerical labelings 1 and 2 in (A–C) are for the compositional profiles 1 and 2 shown in Fig. 6; (E and F) are from another garnet without atoll-structure. Polycrystalline quartz inclusions after coesite occurs in the part of low Mg and high Ca (Grt I) (HP-148). The area outlined by dashed line is Mg-poor part (E). Labeling 3 is for a compositional profile 3 shown in Fig. 6; In X-ray images (G–I), Grt I is associated with omphacite with a polycrystalline quartz inclusion after coesite, and the omphacite has evidently higher Mg content than the matrix omphacite. In the X-ray image of Mg, we can observe some dark domains in Grt I (UD). Labelings 4 and 5 are for the compositional profiles 4 and 5 shown in Fig. 6. (J–L) are from the same garnet without atoll structure (HP-147). Domain CD in Grt I is more Mg rich and Fe poor. Labeling 6 is for the compositional profile 6 shown in Fig. 6. For all X-ray images, black, blue, green, yellow, red and white colors indicate increasing concentration.

Table 2
Representative single spot analysis of minerals for the UHP, HP, EA and GS stages

Samples	HP-147										HP-148		HP-147					HP-148			
Minerals	Grt I and DZ												Grt II								
Features	UD	CD	DZ	UD	CD	DZ	UD	CD	CD	DZ	UD	DZ	Interior	Rim	Interior	Rim		Interior		Rim	RZ
SiO_2	37.55	38.66	38.45	37.87	38.47	38.92	38.44	39.04	38.74	38.90	38.01	38.44	38.32	38.86	39.15	38.80	38.26	38.80	39.19	39.16	38.93
TiO_2	0.06	0.02	0.03	0.05	0.03	0.00	0.11	0.08	0.11	0.10	0.08	0.02	0.00	0.00	0.10	0.05	0.12	0.03	0.00	0.00	0.00
Al_2O_3	21.26	21.94	21.78	21.20	21.74	21.94	21.77	22.10	21.84	22.26	21.26	21.52	21.84	22.14	22.45	22.26	21.77	21.43	21.79	21.79	21.80
Cr_2O_3	0.04	0.04	0.01	0.01	0.03	0.01	0.06	0.02	0.06	0.04	0.01	0.01	0.04	0.30	0.04	0.05	0.00	0.00	0.08	0.01	0.01
FeO	26.49	23.79	25.27	28.02	25.53	24.59	26.93	24.22	26.00	23.94	27.68	26.41	26.73	23.62	24.34	24.52	25.59	25.39	24.64	24.34	26.26
MnO	0.47	0.38	0.37	0.68	0.44	0.50	0.59	0.37	0.42	0.52	0.70	0.67	0.22	0.00	0.42	0.56	0.85	0.38	0.37	0.36	0.63
MgO	3.82	6.41	6.26	2.70	4.85	6.80	3.56	6.24	4.94	6.98	2.87	3.99	5.79	8.78	7.71	8.45	7.39	5.49	7.12	8.28	7.35
CaO	9.81	8.99	7.79	9.51	9.29	7.44	9.26	8.86	9.03	7.62	9.39	9.57	7.27	5.40	6.19	5.39	5.15	8.68	7.12	5.55	5.01
Na_2O	0.04	0.02	0.02	0.01	0.00	0.00	0.00	0.00	0.00	0.00	0.00	0.00	0.01	0.02	0.02	0.00	0.01	0.00	0.00	0.00	0.00
K_2O	0.00	0.00	0.00	0.00	0.00	0.00	0.00	0.00	0.00	0.00	0.00	0.00	0.00	0.00	0.00	0.00	0.00	0.00	0.00	0.00	0.00
Total	99.50	100.21	99.97	100.04	100.35	100.19	100.66	100.91	101.08	100.32	99.99	100.62	100.18	98.82	100.38	100.03	99.14	100.20	100.23	99.48	99.98
O	12	12	12	12	12	12	12	12	12	12	12	12	12	12	12	12	12	12	12	12	12
Si	2.960	2.974	2.978	2.996	2.987	2.998	3.001	2.989	2.988	2.985	3.005	2.995	2.975	2.994	2.995	2.972	2.981	3.011	3.012	3.019	3.011
Ti	0.004	0.001	0.002	0.003	0.002	0.000	0.006	0.005	0.006	0.006	0.005	0.001	0.000	0.000	0.006	0.003	0.007	0.002	0.000	0.000	0.001
Al	1.973	1.988	1.986	1.975	1.988	1.990	2.002	1.992	1.983	2.012	1.979	1.975	1.996	2.009	2.023	2.008	1.998	1.958	1.972	1.978	1.986
Cr	0.002	0.002	0.001	0.001	0.002	0.001	0.004	0.001	0.004	0.002	0.001	0.001	0.002	0.018	0.002	0.003	0.000	0.000	0.005	0.001	0.000
Fe^{3+}	0.000	0.000	0.000	0.000	0.000	0.000	0.000	0.000	0.000	0.000	0.000	0.000	0.000	0.000	0.000	0.000	0.000	0.000	0.000	0.000	0.000
Fe^{2+}	1.746	1.531	1.637	1.854	1.658	1.584	1.759	1.551	1.677	1.536	1.830	1.721	1.735	1.522	1.557	1.571	1.668	1.648	1.584	1.569	1.699
Mn	0.031	0.025	0.024	0.046	0.029	0.033	0.039	0.024	0.027	0.034	0.047	0.044	0.014	0.000	0.027	0.036	0.056	0.025	0.024	0.024	0.041
Mg	0.449	0.735	0.723	0.318	0.561	0.781	0.414	0.712	0.568	0.798	0.338	0.464	0.670	1.008	0.879	0.965	0.858	0.635	0.816	0.952	0.847
Ca	0.828	0.741	0.646	0.806	0.773	0.614	0.775	0.727	0.746	0.626	0.795	0.799	0.605	0.446	0.507	0.442	0.430	0.722	0.586	0.458	0.415
Na	0.006	0.003	0.003	0.002	0.000	0.000	0.000	0.000	0.000	0.000	0.000	0.000	0.002	0.003	0.003	0.000	0.002	0.000	0.000	0.000	0.000
K	0.000	0.000	0.000	0.000	0.000	0.000	0.000	0.000	0.000	0.000	0.000	0.000	0.000	0.000	0.000	0.000	0.000	0.000	0.000	0.000	0.000
Total	8.000	8.000	8.000	8.000	8.000	8.000	8.000	8.000	8.000	8.000	8.000	8.000	8.000	8.000	8.000	8.000	8.000	8.000	8.000	8.000	8.000

HP-147						HP-148		HP-147												
Omp								Brs	Trm	Brs	Brs	Brs	Hbl	Hbl	Act	Phn	Phn	Phn	Pg	
Inc >	Inc >	DZ	Inc <	Matrix	Matrix	Inc >	Matrix	HP-A	HP-A	HP-A	EA-C	HP-A	EA-S	EA-S	GS-S	HP-A	HP-A	HP-A	HP-A	
55.42	54.91	55.15	55.22	56.72	54.86	56.10	56.25	46.62	40.16	49.06	47.25	48.23	50.64	49.45	55.27	54.62	55.58	54.49	48.23	
0.03	0.00	0.03	0.02	0.07	0.04	0.06	0.10	0.20	0.56	0.24	0.12	0.01	0.09	0.04	0.17	0.12	0.21	0.18	0.01	
9.12	10.33	10.08	9.63	10.13	10.11	9.27	10.44	14.01	17.51	12.00	14.30	40.16	4.68	7.29	1.39	23.05	22.89	23.27	40.16	
0.02	0.04	0.02	0.00	0.03	0.00	0.08	0.04	0.01	0.01	0.00	0.01	0.00	0.00	0.01	0.02	0.00	0.04	0.00	0.00	
4.37	4.44	4.83	5.93	4.70	4.90	4.38	4.53	11.82	17.84	10.53	11.89	1.03	12.05	11.68	11.22	1.98	1.79	2.01	1.03	
0.02	0.03	0.00	0.05	0.00	0.03	0.09	0.02	0.10	0.11	0.02	0.06	0.00	0.05	0.19	0.13	0.00	0.01	0.00	0.00	
9.38	8.94	8.32	8.83	8.89	8.90	9.24	8.14	12.6	7.30	13.99	12.10	0.10	15.84	15.02	17.34	4.76	5.04	4.77	0.10	
13.84	13.14	13.24	13.69	13.00	13.45	14.27	13.21	7.84	8.98	8.18	8.71	0.00	12.43	12.18	12.06	0.17	0.01	0.00	0.00	
6.74	7.15	7.08	6.60	7.02	6.78	6.62	7.31	4.16	4.16	3.80	3.63	6.44	0.71	1.47	0.36	0.59	0.35	0.36	6.44	
0.00	0.00	0.00	0.00	0.00	0.00	0.00	0.00	0.28	0.69	0.29	0.19	0.47	0.02	0.10	0.05	9.91	10.12	9.99	0.47	
98.94	98.98	98.75	99.97	100.56	99.07	100.11	100.04	97.63	97.31	98.11	98.25	96.44	96.51	97.42	97.99	95.20	96.04	95.07	96.44	

6	6	6	6	6	6	6	6	23	23	23	23	11	23	23	23	11	11	11	11
1.984	1.959	1.980	1.969	2.000	1.964	1.990	1.993	6.585	5.994	6.854	6.661	3.031	7.319	7.111	7.777	3.619	3.643	3.613	3.031
0.001	0.000	0.001	0.001	0.002	0.001	0.002	0.003	0.021	0.063	0.025	0.013	0.000	0.010	0.004	0.018	0.006	0.010	0.009	0.000
0.384	0.434	0.426	0.404	0.42	0.426	0.387	0.435	2.331	3.077	1.974	2.374	2.972	0.796	1.235	0.23	1.799	1.767	1.817	2.972
0.001	0.001	0.001	0.000	0.001	0.000	0.002	0.001	0.001	0.001	0.000	0.001	0.000	0.000	0.001	0.002	0.000	0.002	0.000	0.000
0.000	0.000	0.000	0.000	0.000	0.000	0.000		0.892	0.601	0.737	0.621	0.000	0.495	0.351	0.435	0.000	0.000	0.000	0.000
0.131	0.132	0.145	0.176	0.139	0.147	0.130	0.134	0.504	1.626	0.493	0.781	0.054	0.962	1.053	0.885	0.110	0.098	0.111	0.054
0.501	0.475	0.445	0.469	0.467	0.475	0.489	0.430	0.012	0.014	0.002	0.007	0.000	0.006	0.023	0.015	0.000	0.001	0.000	0.000
0.001	0.001	0.000	0.002	0.000	0.001	0.003	0.001	2.653	1.624	2.914	2.543	0.009	3.413	3.221	3.637	0.470	0.492	0.471	0.009
0.531	0.502	0.509	0.523	0.491	0.516	0.542	0.501	1.187	1.436	1.224	1.316	0.000	1.925	1.877	1.818	0.012	0.001	0.000	0.000
0.468	0.495	0.493	0.456	0.480	0.471	0.455	0.502	1.139	1.204	1.03	0.992	0.785	0.199	0.41	0.098	0.076	0.044	0.046	0.785
0.000	0.000	0.000	0.000	0.000	0.000	0.000	0.000	0.050	0.131	0.052	0.034	0.038	0.004	0.018	0.009	0.838	0.846	0.845	0.038
4.000	4.000	4.000	4.000	4.000	4.000	4.000	4.000	15.376	15.771	15.306	15.342	6.889	15.127	15.305	14.925	6.930	6.904	6.912	6.889

HP-147

Pg	Ms	Pg	Ky	Zo	Ep	Ep	Ep	Ab	Ab	Olg	Ab	Pmp	Chl	Mrg	Kfs
EA-C	GS-F	GS-F	UHP	UHP	UHP	HP-A	EA-C	EA-C	EA-S	EA-S	GS-S	GS-F	GS-F	GS-F	GS-F
46.90	46.38	48.38	36.95	39.76	38.41	37.90	39.53	65.65	68.26	64.67	66.10	37.42	27.99	33.23	64.71
0.08	0.09	0.10	0.00	0.03	0.19	0.21	0.08	0.02	0.05	0.03	0.01	0.11	0.08	0.13	0.03
40.34	34.40	40.69	63.71	32.03	29.57	26.16	28.79	21.47	19.43	22.36	20.61	25.95	21.50	48.54	19.35
0.00	0.04	0.01	0.01	0.00	0.00	0.02	0.01	0.00	0.01	0.04	0.00	0.00	0.00	0.01	0.00
0.60	0.96	0.55	0.35	2.22	5.03	8.44	6.86	0.32	0.42	0.32	0.30	2.09	14.28	0.53	0.02
0.02	0.04	0.03	0.00	0.00	0.02	0.09	0.09	0.00	0.01	0.00	0.00	0.00	0.05	0.04	0.00
0.12	1.48	0.11	0.02	0.06	0.18	0.07	0.12	0.00	0.17	0.10	0.05	3.73	24.92	0.31	0.06
0.26	0.12	0.45	0.02	23.57	23.33	23.47	23.32	2.30	0.92	3.49	2.02	23.16	0.07	10.00	0.17
7.15	0.05	7.23	0.01	0.00	0.03	0.03	0.00	10.58	11.29	9.92	11.09	0.00	0.00	1.84	1.03
0.68	10.95	0.56	0.02	0.00	0.00	0.00	0.00	0.01	0.02	0.04	0.00	0.05	0.00	0.89	15.15
96.15	94.51	98.11	101.09	97.67	96.76	96.39	98.80	100.35	100.58	100.97	100.18	92.51	88.89	95.52	100.52
11	11	11	5	12.5	12.5	12.5	12.5	8	8	8	8	24.5	14	11	8
2.972	3.111	3.000	0.988	3.030	2.982	2.992	3.014	2.881	2.976	2.831	2.907	5.990	2.734	2.195	2.964
0.004	0.005	0.005	0.000	0.002	0.011	0.012	0.005	0.001	0.002	0.001	0.000	0.013	0.006	0.006	0.001
3.010	2.718	2.972	2.007	2.874	2.703	2.432	2.585	1.110	0.997	1.153	1.067	4.892	2.473	3.776	1.044
0.000	0.002	0.000	0.000	0.000	0.000	0.001	0.001	0.000	0.000	0.000	0.000	0.000	0.000	0.001	0.000
0.000	0.000	0.000	0.000	0.127	0.326	0.557	0.437	0.000	0.000	0.000	0.000	0.000	0.000	0.000	0.000
0.032	0.054	0.029	0.008	0.000	0.000	0.000	0.000	0.012	0.015	0.012	0.011	0.280	1.167	0.029	0.001
0.001	0.002	0.002	0.000	0.000	0.001	0.006	0.006	0.000	0.000	0.000	0.000	0.000	0.004	0.002	0.000
0.011	0.148	0.010	0.001	0.007	0.021	0.008	0.014	0.000	0.011	0.007	0.003	0.890	3.629	0.031	0.004
0.018	0.009	0.030	0.001	1.924	1.941	1.985	1.905	0.108	0.043	0.164	0.095	3.972	0.007	0.708	0.008
0.879	0.007	0.869	0.001	0.000	0.005	0.005	0.000	0.900	0.954	0.842	0.946	0.000	0.000	0.236	0.091
0.055	0.937	0.044	0.001	0.000	0.000	0.000	0.000	0.001	0.001	0.002	0.000	0.010	0.000	0.075	0.885
6.982	6.993	6.961	3.007	7.964	7.990	7.998	7.967	5.013	4.999	5.012	5.029	16.047	10.020	7.059	4.998

All Fe as Fe^{2+} for garnet and omphacite; the Fe^{3+} estimate of amphibole by the stoichiometric constraint of $T+C=13$ excluding Ca, Na and K at the *T* and *C* sites; UD, CD, DZ and RZ, see Figs. 3, 5 and 6; Interior-rim: from the interior to the rim of Grt II; Inc >: omphacitic inclusions in Grt I with >300 μm in size; Inc <: omphacitic inclusions in Grt I with <100 μm in size; matrix: Omp in matrix; HP-A: coexisting with Grt II; EA-C: coarse-grained assemblage in the EA stage; EA-S: symplectitic assemblage in the EA stage; GS-S: symplectitic assemblage in the GS stage; GS-F: assemblage developed along the fractures; UHP: minerals in the UHP stage; Brs: barroisite; Trm: taramite; Olg: oligoclase; Phn: phengite, and other mineral abbreviations are from Kretz (1983).

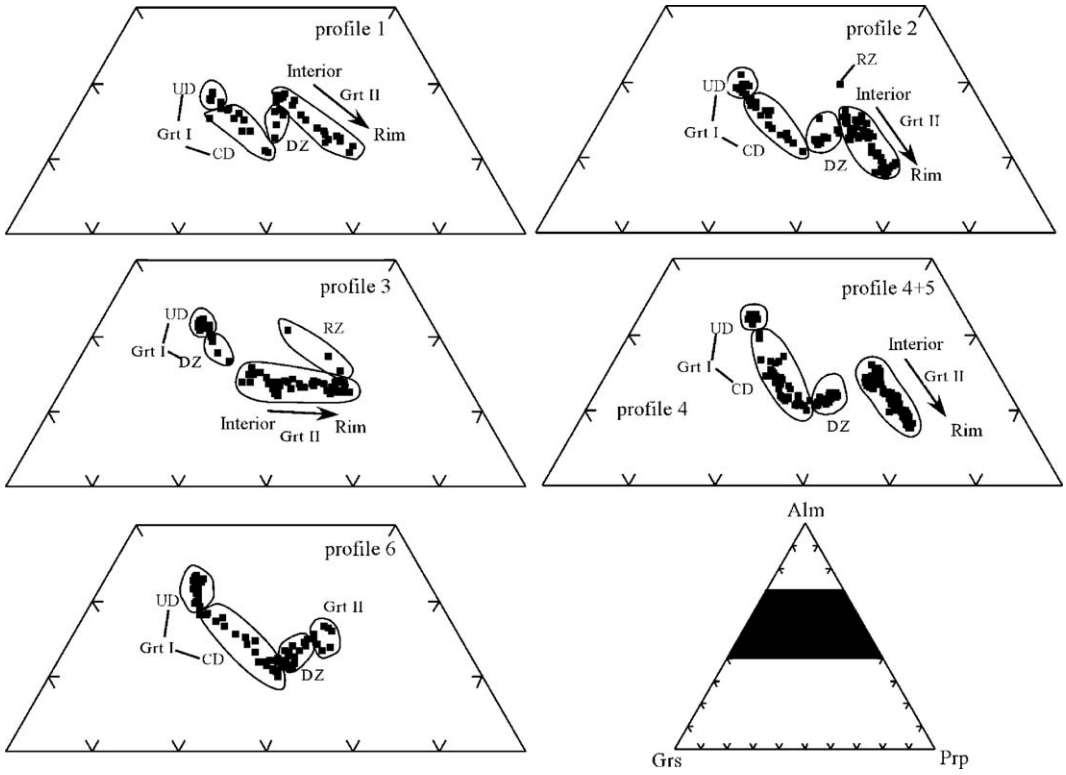

Fig. 5. Endmember plot of garnet of 6 compositional profiles. Grs: grossular; Alm: almandine; Prp: pyrope. UD: relict patchy Mg-poor and Fe-rich domain in Grt I; CD: Mg-rich and Fe-poor domain in Grt I; DZ: transitional compositional zone between Grt I and Grt II. RZ: Mg-poor and Fe-rich zone of 5–25 μm width in the outermost rim of Grt II.

conditions, whereas the composition of domain CD experienced variable modification (Figs. 3, 5 and 6). The degree of substitution differs significantly in different garnet grains, e.g., the substitution is not observed in the Grt I in Fig. 3E, whereas the highest degree of substitution of Mg for Fe^{2+} is usually developed in the rim parts of Grt I.

Grt II shows an increase of Mg from the interior to the rim at the expense of Fe (profiles 2 and 5, Fig. 6) or Ca (profiles 3, Fig. 6) or Fe and Ca (profile 1, Fig. 6), which is also demonstrated in pyrope–almandine–grossular triangle diagrams (Fig. 5). The compositional zoning of Grt II shows a consistent change from the interior to the rim, which can be interpreted as growth zoning (Spear, 1993). Grt II at different sites also show different growth processes. Most Grt II started to grow with a similar composition (profiles 2, 4+5, 6, Fig. 5), but some began their growth at the composition with a higher Fe^{2+}/Mg ratio (profile 1, Fig. 5). It is worth noting that the Grt II of profile 6 (Figs. 3J, 5 and 6) is narrow from the interior to the rim, and hardly developed a compositional zoning like other grains of Grt II. This may indicate that this overgrowth ceased to grow at an earlier time than other Grt II.

Domain DZ is located between Grt I and Grt II (Fig. 3). The composition of DZ is clearly distinguished from that of CD in Fig. 5 although it is not clear in the X-ray images (Fig. 3) and compositional profiles (Fig. 6). Because the compositions of DZ are between the rim part of Grt I and the interior rim of Grt II (Fig. 5), DZ can be interpreted to be formed by the volume diffusion between Grt I and Grt II. This compositional relationship also clearly indicates that the UHP Grt I experienced a compositional change through Mg substituting Fe^{2+} prior to the overgrowth of Grt II-related assemblages at the HP stage.

Omphacite is heterogeneous in compositions, but it does not display compositional zoning like garnet. Therefore, it is more difficult to interpret the compositional heterogeneity. Fortunately, X-ray compositional images provide a possible solution for understanding the evolution of omphacite in the metamorphic process (Fig. 3E, G and J). Omphacite inclusions of >300 μm diameter are enclosed in Grt I (Fig. 3E, G and J). The identification of a polycrystalline quartz inclusion after

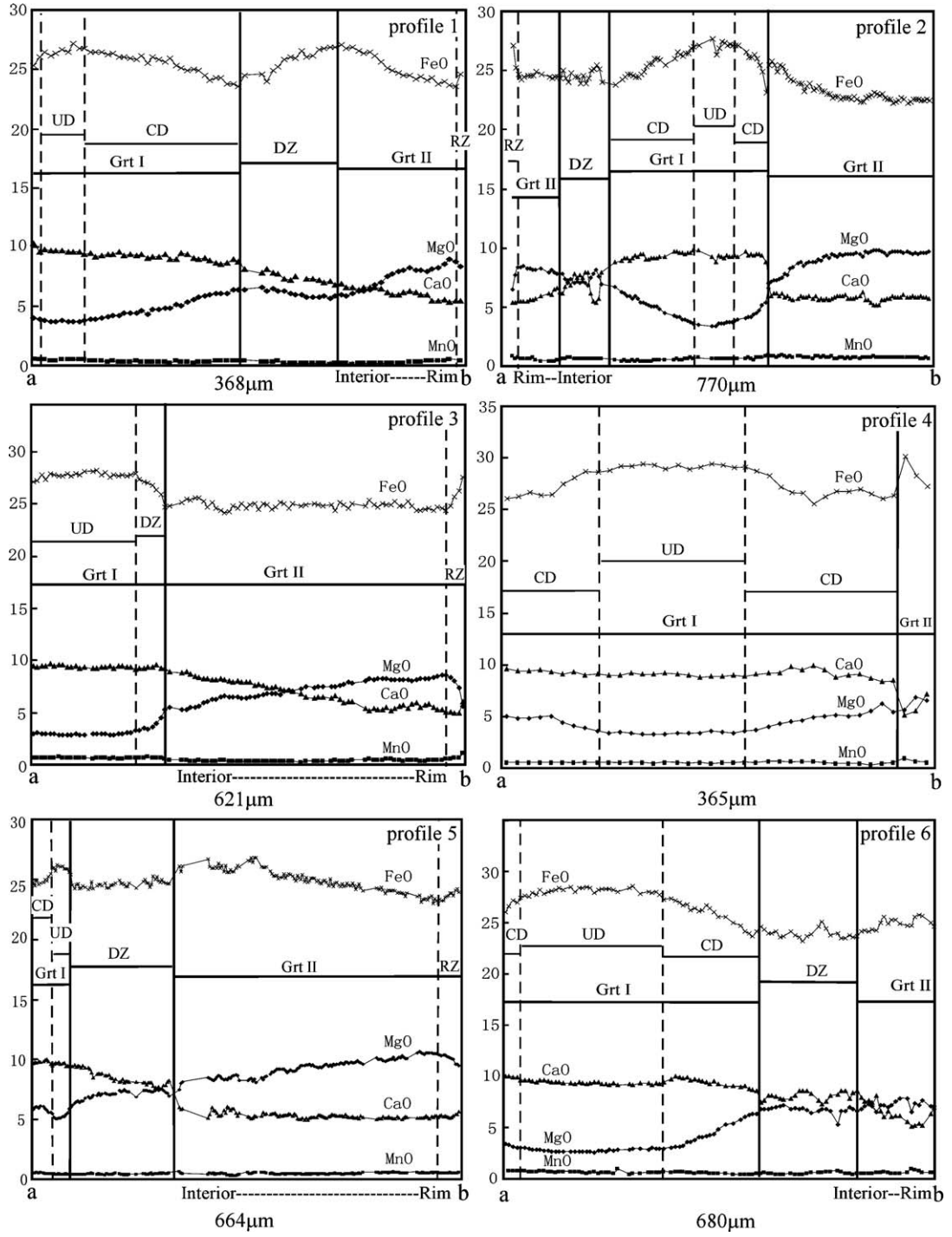

Fig. 6. Compositional profiles of garnets. UD: relict patchy Mg-poor and Fe-rich domain in Grt I; CD: Mg-rich and Fe-poor domain in Grt I; DZ: transitional compositional zone between Grt I and Grt II. RZ: Mg-poor and Fe-rich zone of 5–25 μm width in the outermost rim of Grt II. inner—outer: from inner to outer rims for Grt II.

coesite in one of these omphacite inclusions (Fig. 3G) suggests that these omphacite inclusions formed at the UHP stage, and possibly preserve as an original composition equilibrated at that stage. These omphacite inclusions show systematically higher Mg content and lower Fe^{2+}/Mg ratio than omphacite in the matrix (Figs.

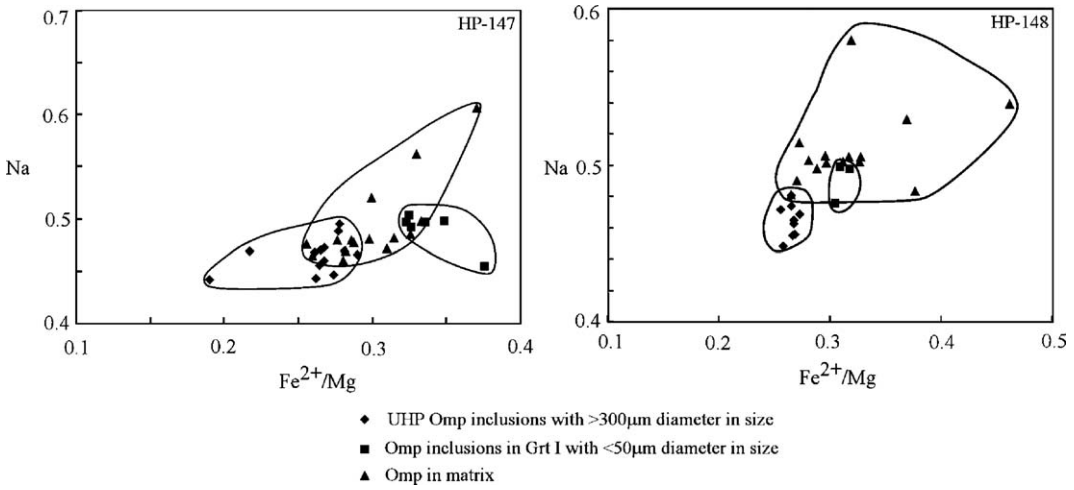

Fig. 7. Na–Fe^{2+}/Mg plot of omphacite. Total Fe is assigned to Fe^{2+}. Omphacite inclusion of >300-μm size shows systematically lower Fe^{2+}/Mg ratios than the inclusion of <50 μm and omphacite in the matrix.

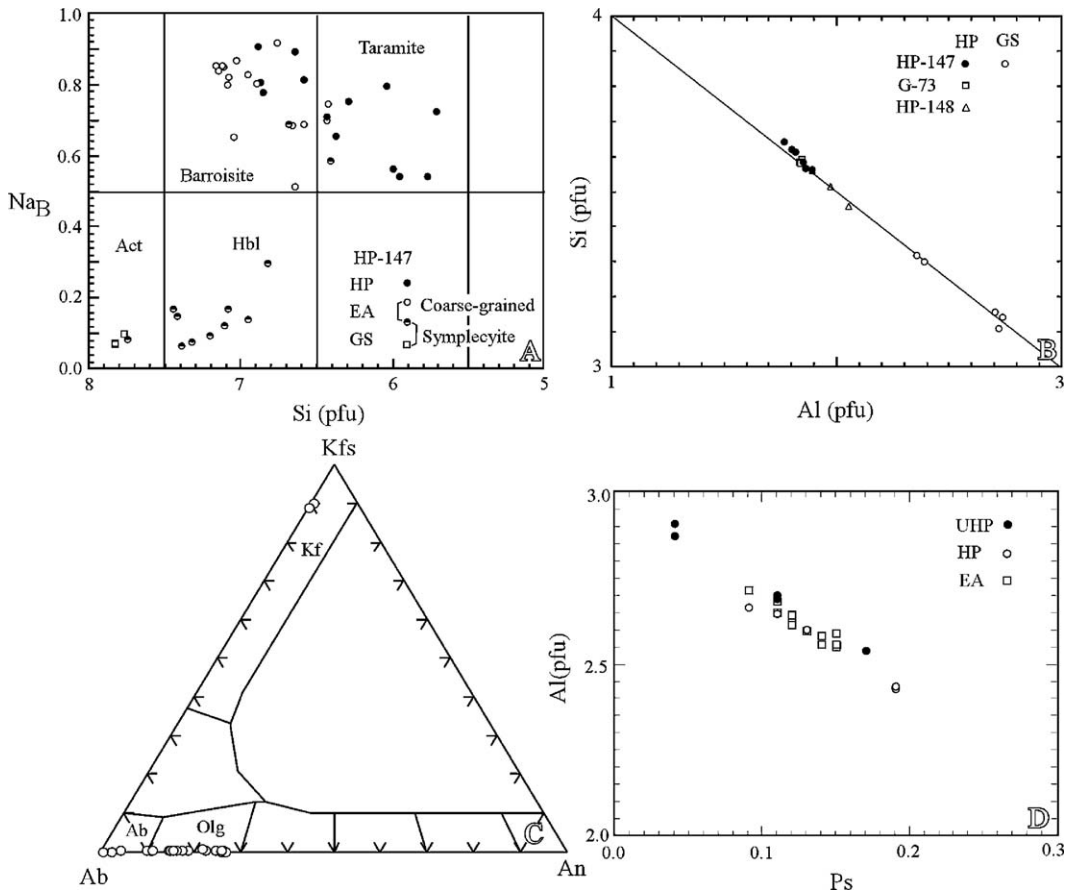

Fig. 8. (A) amphibole classification (Leake et al. 1997). Na_A and Na_B: Na content at A and B-sites; Si: Si content at T-site. Taramite is the amphibole with $Na_A \geq 0.5$ and $0.5 < Na_B < 1.5$. HP: amphiboles formed at the HP stage; EA: amphiboles at the EA stage; GS: amphiboles formed at the GS stage. (B) Si vs. Al relation for phengite. HP: phengite formed at the HP stage; GS: phengite or muscovite at the GS stage. (C) endmember plot for plagioclase formed at the EA and GS stages. (D) Al vs. Ps (Fe/(Fe+Al)) plot for epidote group minerals.

3E, G, J and 7), indicating that omphacite composition in the matrix had been modified to different degrees during the substitution of Mg for Fe^{2+} of Grt I. This can easily be interpreted as a result of Fe^{2+}–Mg exchange reaction between garnet and omphacite. The Fe^{2+}–Mg exchange reaction can also be observed in the X-ray image of Fig. 3G: a 50 to 100 μm wide zone in omphacite inclusion along its contact with Grt I (Fig. 3G) shows a decreasing Mg content and increasing Fe content, and the garnet along this contact shows a reverse changes of compositions (see the left end in profile 4 of Fig. 6). Therefore, these observations indicate that Fe^{2+}–Mg exchange between omphacite and Grt I is an important process in response to the change of *P–T* condition in the exhumation of the UHP rocks. In addition, it is worth noting that the Fe^{2+}–Mg exchange between omphacite and Grt I occurred in a 50 to 100 μm zone, therefore omphacite inclusions smaller than this size generally do not preserve their original compositions, as indicated by their higher Fe^{2+}/Mg ratio (Fig. 7).

Omphacite in the matrix has higher Na content than omphacite inclusion in Grt I. This compositional difference cannot be explained by Fe^{2+}–Mg exchange reaction alone between garnet and omphacite. The Grt II-related assemblages represent the products of some net transfer reactions at the expense of UHP assemblage and fluids (Fig. 3). Therefore, the compositional variation of omphacite should also be associated with formation of the Grt II-related assemblage. We will further discuss this question in Section 5.4.

5.2. Exhumation *P–T* path of the UHP eclogite

The four generations of mineral assemblages in the Hong'an samples are used to determine *P–T* conditions from the UHP, via HP and EA, to GS stages. These *P–T* estimates are then used to construct a *P–T* path of the UHP rocks exhumation.

The amount of Fe assigned to Fe^{3+} in garnet and omphacite is sensitive to temperature estimation when the Fe^{2+}/Mg exchange thermometer is used for the Grt–Cpx mineral pair. Because omphacite has a low Fe content and Na > Al, all Fe is assigned to Fe^{2+} when this mineral has < 4.5% FeO; otherwise Fe^{2+} was estimated using the average value between Fe^{2+} = total Fe and Fe^{2+} = total Fe–Fe^{3+}, where Fe^{3+} = Na–Al. For garnet, all Fe is assigned to Fe^{2+} for the *P–T* estimation.

5.2.1. UHP stage

The UHP temperature of metamorphism was estimated by using the Fe^{2+}/Mg exchange Grt–Cpx thermometer (Krogh Ravna, 2000) (Table 3). We used the UD domain in Grt I (Figs. 3, 5 and 6) and > 300 μm omphacite inclusions (Fig. 3) to calculate *P–T* conditions of this stage. Since these omphacite inclusions all have < 4.5% FeO, total Fe was assigned to Fe^{2+}. Therefore, the estimated temperature represents a maximum temperature. Because diamond was not identified in the UHP rocks in the Hong'an area,

Table 3
Results of *P–T* estimate for the UHP, HP and EA stages

Stages	Samples	Some parameters, thermobarometers and results				Average results
		Grt–Cpx thermometer (Krogh Ravna, 2000)				
UHP	HP-147	K_d	X_{Ca} (Grt)	2.5 GPa	3.0 GPa	2.8 GPa, 520 °C
		18.85	0.265	510	530	
		18.57	0.265	514	534	
		19.57	0.265	503	523	
		21.45	0.255	483	502	
		20.68	0.273	502	522	
	HP-148	19.02	0.274	534	554	
		20.37	0.282	534	554	
Intersections between Grt–Cpx–phn barometer (Waters and Martin, 1993) and Grt–Cpx thermometer (Krogh Ravna, 2000)						
HP	HP-147	K_d	S i (Phn)	T (°C)	P (GPa)	1.80±0.06 GPa 634±37 °C
		6.72	3.59	605	1.75	
		7.29	3.64	575	1.80	
		5.08	3.64	685	1.85	
		5.85	3.61	640	1.80	
		5.65	3.62	670	1.80	
		7.33	3.62	585	1.65	
	G-73	6.08	3.59	647	1.85	
		6.39	3.59	617	1.75	
		5.96	3.58	658	1.85	
		5.69	3.58	658	1.80	
Intersections between the Ed–Tr and Ed–Ri thermometers, Amp–Pl thermometer (Holland and Blundy, 1994)						
HP-147	Ep Amp	Si (Amp)	X_{Ab} (Pl)	T (°C)	P (GPa)	0.74±0.23 GPa 568±44 °C
		7.20	0.82	537	0.68	
		7.10	0.82	550	1.0	
		7.00	0.89	584	0.63	
		7.47	0.89	555	0.61	
		7.43	0.89	570	0.71	
		7.09	0.84	614	1.0	
		6.96	0.84	638	1.0	
		7.09	0.84	640	0.86	
		7.15	0.77	500	0.44	
		7.15	0.84	548	1.0	
		7.15	0.78	539	0.51	
		7.15	0.78	535	0.43	

Si (Phn): Si value per formula of phengite; Si (Amp): Si value per formula of amphibole; X_{Ca}(Grt) = Ca/(Ca + Fe^{2+}Mg + Mn); X_{Ab}: albite content in plagioclase;
$K_d = (Fe^{2+}/Mg)_{Grt}/(Fe^{2+}/Mg)_{Omp}$.

coesite may have grown in the graphite-stability field, and thus the pressure of UHP stage can be confined by the stability limits of graphite and coesite (Fig. 9). Using this approach the temperatures and pressures were estimated to be about 480–560 °C and 2.4 to 2.9 GPa with median values of 520 °C and 2.8 GPa, respectively.

5.2.2. HP stage

The *P–T* conditions of the HP assemblage was estimated by using the Grt–Omp–Phn barometer (Waters and Martin, 1993, revised 1996) and the Fe^{2+}/Mg exchange Grt–Cpx thermometer (Table 3). Grt II, and associated omphacite and phengite are used to calculate the *P–T* conditions. The results show that

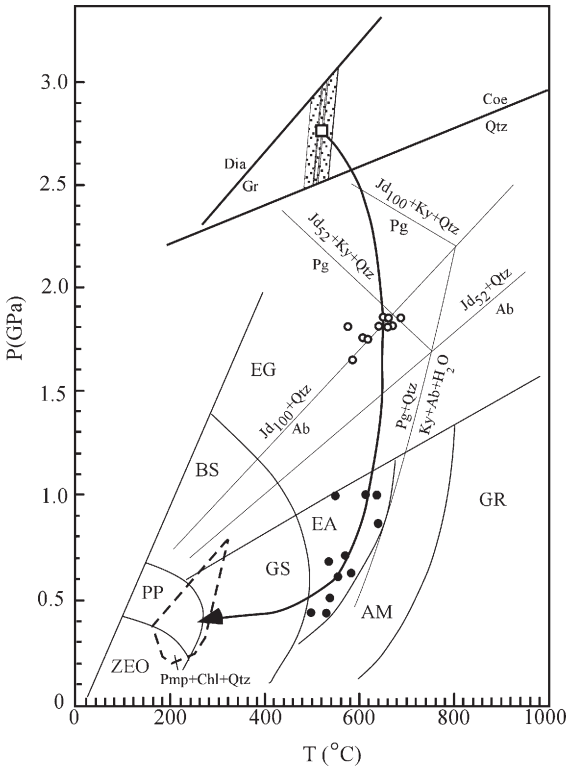

Fig. 9. *P–T* conditions estimated for all stages and *P–T* path of exhumation of UHP eclogite in the Hong'an area. Dotted area is the *P–T* estimate for the UHP stage, and the square represents the median value of the *P–T* estimates. The fine lines are the *P–T* conditions calculated by the Fe^{2+}–Mg exchange garnet-omphacite thermometer of Krogh Ravna (2000). The stable field of pumpellyite + chlorite + quartz outlined by the thick dashed line is based on Frey et al. (1991). The grid of metamorphic facies is based on Spear (1993). The reactions labeled were calculated using the internally consistent thermodynamic data (Holland and Powell, 1998). GR: granulite facies; AM: amphibolite facies; EA: epidote amphibolite facies; GS: greenschist facies; PP: prehnite–pumpellyite facies; ZEO: zeolite facies; BS: blueschist facies; EG: eclogite facies.

temperature and pressure range from 575 to 685 °C and 1.6 to 1.9 GPa, with average values of 634±37 °C and 1.8±0.06 GPa, respectively (Fig. 9). These *P–T* estimates fall within the stability field of omphacite (Jd_{42-52})+paragonite and omphacite+quartz, which is consistent with the fact that paragonite grew at this stage.

5.2.3. EA stage

We have estimated the *P–T* conditions of the EA stage by using the amphibole–plagioclase thermometer (Holland and Blundy, 1994) (Table 3). The assemblages include the coarse-grained assemblage of amphibole+epidote+paragonite+quartz+albite–oligoclase and symplectite of plagioclase+amphibole after omphacite. Besides albite, the rock contains plagioclase with Ab contents between 73 and 89 mol%. Those plagioclases and coexisting amphiboles can be used to calculate the *P–T* conditions employing the edenite–richterite and edenite–tremolite thermometers (Holland and Blundy, 1994). The intersection between the two thermometers yields temperatures of 500 to 640 °C and pressure of 0.4 to 1 GPa for this stage, which plots in the field of the epidote amphibolite facies (Fig. 9).

5.2.4. GS stage

No thermometer or barometer could be used to determine the *P–T* conditions of this stage because of a lack of appropriate mineral assemblages. For the assemblage pumpellyite+muscovite+chlorite+margarite+albite+K-feldspar+epidote+quartz, we used the petrogenetic grid of Frey et al. (1991) to constrain the possible *P–T* conditions (Fig. 9). In the system Na_2O–CaO–MgO–Al_2O_3–SiO_2–H_2O, the assemblage of pumpellyite+chlorite+quartz is stable within a field of 160 to 320 °C and 0.2 to 0.8 GPa, which approximately constrains the *P–T* conditions for the GS stage.

The above *P–T* estimates of the different stages define an uplift trajectory consisting of three segments (Fig. 9): a segment of initial temperature increase of >100 °C from the UHP to HP stages, a segment of approximately isothermal decompression from the HP to EA stages, and a segment of dramatic temperature decrease from the EA to GS stages.

5.3. Implications of P–T path

Previous studies have shown that garnet from UHP eclogites from Hong'an area is characterized by compositional zoning defined by an increase in Mg and decrease in Ca and Fe from core to rim (e.g., Zhang and Liou, 1994; Liu et al., 2004). The

composition of the high Mg rim was used to estimate peak UHP conditions of 620–670 °C and 2.6–3.1 GPa (Liu et al., 2004; Zhang and Liou, 1994). However, this study reveals that garnet was formed at two different metamorphic stages (UHP and HP), and that only Grt I can be used to estimate *P–T* conditions for UHP metamorphism, although it has lower Mg and higher Ca contents than Grt II.

As discussed above (Section 5.1), garnet shows complicated compositional zoning patterns. Therefore, it is a key issue to correlate the UHP metamorphic event with a compositional domain in garnet zoning. The X-ray compositional mapping for minerals is critical and necessary for such correlation. Another excellent example in our study is also from the observation on sample HP-199. Garnet in this sample displays complicated patchy compositional structure (Fig. 10). A coesite inclusion was found in a Mg-poor and Ca-rich patch, indicating its formation at peak pressure. In contrast, the high Mg patches have high Mg/Fe^{2+} ratios, recording a higher temperature than the high Ca domain. Therefore, we are able to avoid the great uncertainty arising from previous *P–T* estimates of the UHP metamorphism in the Hong'an area because of the lack of an appropriate interpretation on garnet zoning on the basis of X-ray compositional mapping.

The shape of the *P–T* path related to exhumation reflects the rate of tectonically-driven exhumation relative to the rate of thermal relaxation and re-equilibration of the subducted crustal slab. Unless the uplift rate is exceedingly fast, deeply subducted rocks may continue to experience heating in the early stages of exhumation. Therefore, the maximum subduction depth would be reached before the rocks attained their maximum temperature that would be achieved at a shallower depth along the exhumation path (Carswell and Zhang, 2000). The *P–T* path shows that the UHP eclogite in the Hong'an area was not isothermally uplifted in the early stage of exhumation from UHP to 1.8 GPa pressures (Fig. 9), implying a relatively slow uplift rate in the stage. The slow uplift results in heating of UHP rocks with >100 °C. In fact, the diffusion modification of Grt I induced by Fe^{2+}–Mg exchange reaction with omphacite also suggests a relatively slow uplift rate. The diffusion occurred at the temperature of 520 to 640 °C. The X-ray compositional images (e.g., Fig. 3J) show that the diffusion zones of Mg and Fe^{2+} are >100 μm in size. The diffusion zone of pre-existing garnet during exhumation is generally limited to tens of microns, e.g., the diffusion zone is about 10 to 20 μm in garnet of eclogite from the Tauern Window (Dachs and Proyer, 2002) and Yukon–Tanana terrane (Perchuk et al., 1999), which formed at similar temperatures with our samples. At approximately the same temperature, our case suggests no doubt a relatively slow uplift rate in the early stage of exhumation. The diffusion size between Grt I and II has a range from 40 to 70 μm along profiles 1 and 3 (Fig. 6), and this scale indicates faster exhumation than that of the first stage.

One important aspect for constructing metamorphic *P–T* path is how to unravel the re-equilibration of the early mineral assemblage during subsequent exhumation-related processes. The UHP eclogites from Hong'an experienced a maximum temperature of about 680 °C. Under such conditions of temperature conditions, we have observed the UHP garnet and omphacite were variably modified in their compositions by Fe^{2+}–Mg exchange, and the original compositions of garnet equilibrated at the UHP stage are only preserved in some domains in Grt I. Moreover, for small omphacite inclusions (e.g., <100 μm), their composition would have been seriously modified through exchange of Fe^{2+}–Mg with garnet. If the omphacite inclusions formed during subduction and such modified compositions were used, this would inevitably result in unrealistically high temperature estimates, and therefore result in very tight, hairpin-style, *P–T*–time paths. As pointed out by Carswell and Zhang (2000), this kind of *P–T–t* path may be an unrealistic representation of the actual paths that the rocks underwent. The UHP eclogites in the eastern Dabie and Sulu areas experienced temperatures in excess of 700 °C (e.g., Wang et al., 1992; Wang et al., 1993; Zhang et al., 1995a,b; Carswell et al., 1997; Tabata et al., 1998; Nakamura and Hirajima, 2000; Schmid et al., 2000, 2003). If the size of garnet and omphacite are not coarse enough, we may expect that mineral compositions equilibrated at the condition of peak pressure have probably been seriously modified in the subsequent processes so that geothermobarometric studies of these rocks can give peak temperatures but not peak pressures. Therefore, we think that *P–T* estimates for the UHP eclogites in eastern Dabie and Sulu areas represent the *P–T* conditions near peak temperature rather than near peak pressure.

The temperature estimated for the peak UHP pressure for the Hong'an samples in this study is unusually low for the studied samples, which may leads suspicion that temperatures were underestimated. However, because total Fe was assigned to Fe^{2+} for the UHP omphacite in our study, the temperature should not be significantly underestimated. Our results

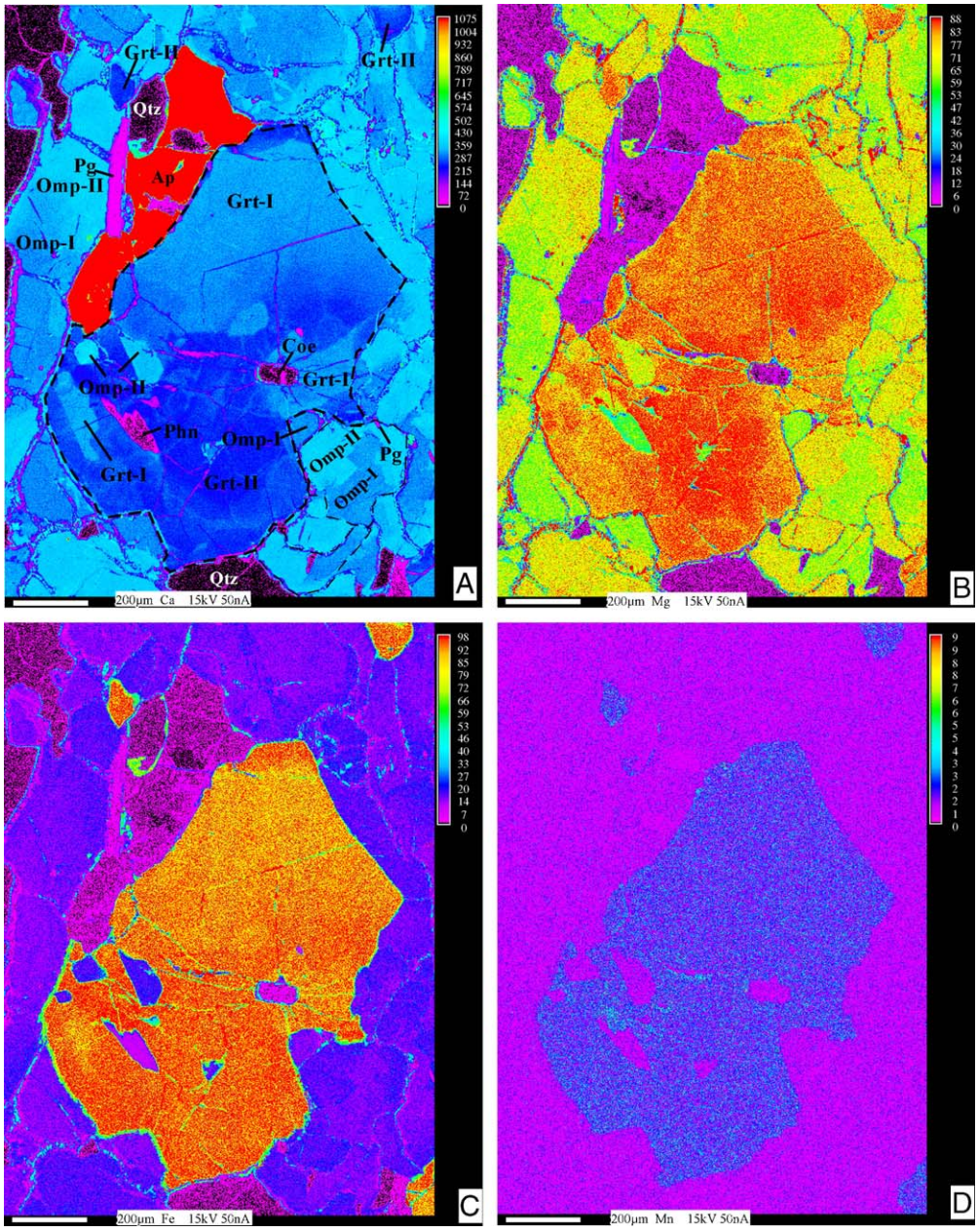

Fig. 10. X-ray images showing garnet zoning (HP-199). Garnet shows patchy zoning. Ca-rich and Mg-poor patches (Grt-I) formed in an early stage and have coesite inclusion. Low Mg content of these patches indicates that they formed at lower temperature condition but at peak pressure condition. Grt II coexists with phengite. Omphacite also formed in two stages: the early one (Omp-I) is Na- and Al-rich, whereas the late one (Omp-II) is Fe-, Mg- and Ca-rich. The late omphacite is associated with paragonite.

indicate a geothermal gradient in the order of 5–6 °C/km (assuming 3.3 km/0.1 GPa), consistent with two recent petrologic studies of UHP eclogites in the eastern Dabie Mountains (Schmid et al., 2003; Proyer et al., 2004). When ferric iron is actually determined by Micro-XANES and Mössbauer spectroscopy, the *P–T* estimates give the same geothermal gradient (Schmid et al., 2003; Proyer et al., 2004). These results, if reliable, imply that the subduction rate of continental slab was very fast so that the temperature at the UHP conditions was very low.

5.4. Metamorphic fluids

The presence of metamorphic fluids during retrograde process has been manifested by the growth of

hydrous minerals such as amphibole, epidote, phengite, muscovite, and paragonite in the Hong'an samples. On the basis of mineral assemblages, we can infer some important features of the fluids, such as K content.

In the studied samples, the UHP assemblage was inferred to be Grt I+Omp+Ky+Zo/Ep+Coe. The epidote group minerals are the only hydrous phases that coexist with Grt I under the UHP condition. Phengite has been regarded as a common phase for the UHP assemblage in previous studies (e.g., Zhang and Liou, 1994). However, in our samples it is clear that phengite is secondary and only occurs in atoll Grt II-related assemblages that are variable in different domains (Table 1). The pressure estimates of 1.6 to 1.9 GPa for these assemblages indicate that they formed during the exhumation process after the UHP metamorphism. If the change of mineral assemblages from the UHP to HP stages happened in a closed system, a precursor K-phase for phengite is also necessary. Such a precursor phase has not been identified in the UHP assemblage. Therefore, influx of fluids must have been involved in the formation of significant amount of hydrous minerals in HP Grt II-related assemblages, and the fluids provided K and volatile components for phengite, paragonite, amphibole and epidote. For the formation of atoll Grt II-related assemblage, a possible reaction is Cpx I+Grt I+Ky+K-rich fluid=Grt II+Cpx II++Phn+Ep+Pg+Qtz. The Grt II-related assemblage replaces Grt I (Fig. 3), suggesting that Grt I is a reactant phase. Kyanite, as a relict phase in epidote, also indicates that it was involved in the reaction as a reactant. In the reaction, Cpx I can be represented by the omphacite inclusion in Grt I, and Cpx II by the matrix omphacite. The compositional difference between Cpx I and II suggests that the reaction mainly consumes the diopside component of Cpx I since Cpx II has higher jadeite content. At the same time, the higher Mg content of Grt II may also be explained by the higher Fe^{2+}/Mg of Cpx II, and the lower Ca content of Grt II can be explained by formation of epidote and amphibole in this reaction. This reaction was clearly driven by influx of K-rich fluids.

In fact, some previous researches have shown the presence of K-rich fluids in HP and UHP metamorphism. The minute polyphase inclusions of microdiamond, phlogopite, quartz, paragonite, phengite, apatite, and rutile in garnet of ultrahigh-pressure metamorphic gneiss of the Erzgebirge are interpreted to represent original inclusions of a supercritical dense COH fluid rich in K, Na, and SiO_2 (Stöckhert et al., 2001). Metasomatism with K-rich fluids was reported for fine grained rodingite-like rocks from the high-pressure metamorphic Maksyutovo Complex in the Southern Urals (Schulte and Sindern, 2002), eclogites from the Marun–Keu complex of Polar Urals (Molina et al., 2002), and eclogites from the Franciscan Complex, California, and related terranes of Oregon and Baja California, and from the Samana Metamorphic Complex, Samana Peninsula, Dominican Republic (Sorensen et al., 1997). Phengite is always involved in this K-rich fluids metasomatism. In addition, mass balance calculation requires the involvement of K-rich fluids in an eclogite facies shear zone in a metapelite of the Monte Rose nappe, western Alps (Keller et al., 2004). Therefore, K-rich fluids probably are widely involved in HP and UHP metamorphic process. Likely sources of K-rich fluids are from formation or decomposition reactions of phengite, as have been described in some phengite-related high-pressure experiments (Massonne, 1992; Schmidt, 1996; Wunder and Melzer, 2003). The high-pressure experiment by Massonne (1992) show that phologopite+K-feldspar+H_2O can react to produce phengite±quartz+K, Mg-rich siliceous fluid at the conditions of above 1.5 GPa and 400 to 700 °C. This reaction is possibly responsible for formation of phengitic mica in gneissic rocks. A speculation is that K-rich fluids should be widely present in subducted continental slab with >1.5 GPa depth due to the above reaction, and make up a zone of K-rich fluids at such depths. When UHP rocks exhume to such depths, some eclogites absorb such fluids to produce phengite-bearing assemblages, as observed in our samples. However, there is still an alternative interpretation. The temperatures at HP stage are close to the wet solidus in felsic systems. It is possible to produce a hydrous melt at such conditions. If this is the case, hydrous felsic melts could interact with the eclogites to produce the observed metasomatism. A proof against this interpretation is that any phenomenon of partial melting, such as leucosome, does not be observed in country gneisses of the eclogites. Therefore, we prefer the first interpretation.

Phengite is not present in the EA assemblages, indicating that the fluids were K-poor at that stage. GS assemblages formed along fractures, and muscovite/phengite and K-feldspar are common phases, implying that the fluids became K-rich again at this stage.

6. Conclusions

UHP eclogites from the Hong'an area were overprinted by a series of metamorphic events in the process

of their exhumation. This study gives the following significant results:

1. X-ray mapping and textural observation identified four generations of mineral assemblage formed at the UHP, HP, EA and GS stages, respectively. UHP and HP garnets have significantly different compositions, and UHP garnets were variably modified in composition by Fe–Mg exchange with omphacite and volume diffusion between UHP and HP garnets.
2. *P–T* estimates demonstrate that UHP eclogites experienced a temperature increase of over 100 °C from the UHP to HP stages. This challenges the conventional assumption that UHP rocks synchronously achieved maximum temperatures and pressures. The UHP rocks experienced an approximately isothermal depression from the HP to EA stages, followed by significant cooling from the EA to GS stages.
3. In the process of exhumation, UHP eclogites experienced a series of episodes of fluid–rock interaction, resulting in the formation of hydrous minerals. Hydrous mineral compositions suggest that the nature of fluids was different in different stages: K-rich at the HP stage, K-poor at the EA stage, and K-rich again at the GS stage.

Acknowledgements

We thank Ping Xu and Yuguang Ma for their assistance in probe analysis. Three anonymous reviewers are thanked for their constructive reviews that significantly improved this study. This research was financially supported by the Natural National Science Foundation of China (Project 40272037, 40421202) and by grants from Knowledge Innovating Project of Chinese Academy of Sciences (KZCX3-SW-135) and from Chinese National Key Projects (G1999075501).

References

Ames, L., Tilton, G., Zhou, G., 1993. Timing of collision of the Sino–Korean and Yangtse cratons: U–Pb zircon dating of coesite-bearing eclogites. Geology 21, 239–242.

Banno, S., Enami, M., Hirajima, T., Ishiwatari, A., Wang, Q.C., 2000. Decompression *P–T* path of coesite eclogite to granulite from Weihai, eastern China. Lithos 52, 97–108.

Carswell, D.A., Zhang, R.Y., 2000. Petrographic characteristics and metamorphic evolution of ultrahigh-pressure eclogites in plate-collision belts. In: Ernst, W.G., Liou, J.G. (Eds.), Ultra-High Pressure Metamorphism and Geodynamics in Collision-Type Orogenic Belts. Geological Society of America, vol. 4. Bellwether Publishing, Ltd., pp. 39–56.

Carswell, D.A., O'Brien, P.J., Wilson, R.N., Zhai, M., 1997. Thermobarometry of phengite-bearing eclogites in the Dabie Mountains of central China. J. Metamorph. Geol. 15, 239–252.

Cui, W.Y., Wang, X.Y., 1995. Eclogites of southern Henan and northern Hubei Provinces, central China. Isl. Arc 4, 347–361.

Dachs, E., Proyer, A., 2002. Constraints on the duration of high-pressure metamorphism in the Tauern Window from diffusion modelling of discontinuous growth zones in eclogite garnet. J. Metamorph. Geol. 20, 768–780.

Eide, E.A., Liou, J.G., 2000. High-pressure blueschists and eclogites in Hong'an: a framework for addressing the evolution of high- and ultrahigh-pressure rocks in central China. Lithos 52, 1–22.

Eide, E.A., McWilliams, M.O., Liou, J.G., 1994. $^{40}Ar/^{39}Ar$ geochronology and exhumation of high-pressure to ultrahighpressure metamorphic rocks in east central China. Geology 22, 601–604.

Frey, M., De Capitani, C., Liou, J.G., 1991. A new petrogenetic grid for low-grade metabasites. J. Metamorph. Geol. 9, 497–509.

Hacker, B.H., Ratschbacher, L., Webb, L., Ireland, T., Walker, D., Dong, S., 1998. U–Pb zircon ages contain the architecture of the ultrahigh-pressure Qinling–Dabie Orogen, China. Earth Planet. Sci. Lett. 161, 215–230.

Holland, T.J.B., Blundy, J.D., 1994. Non-ideal interactions in calcic amphiboles and their bearing on amphibole–plagioclase thermometry. Contrib. Mineral. Petrol. 116, 433–447.

Holland, T.J.B., Powell, R., 1998. An internally-consistent thermodynamic dataset for phases of petrological interest. J. Metamorph. Geol. 16, 309–344.

Keller, L.M., Abart, R., Stunitz, H., De Capitani, C., 2004. Deformation, mass transfer and mineral reactions in an eclogite facies shear zone in a polymetamorphic metapelite (Monte Rosa nappe, western Alps). J. Metamorph. Geol. 22, 97–118.

Kretz, R., 1983. Symbols for rock-forming minerals. Am. Mineral. 68, 277–279.

Krogh Ravna, E., 2000. The garnet–clinopyroxene Fe^{2+}–Mg geothermometer: an updated calibration. J. Metamorph. Geol. 18, 211–219.

Leake, B.E., Woolley, A.R., Arps, C.E.S., Birch, W.D., Gilbert, M.C., Grice, J.D., Hawthorne, F.C., Kato, A., Kisch, H.J., Krivovichev, V.G., Linthout, K., Laird, J., Mandarino, J.A., Maresch, W.V., Nickel, E.H., Rock, N.M.S., Schumacher, J.C., Smith, D.C., Stephenson, N.C.N., Ungaretti, L., Whittaker, E.J.W., Guo, Y.Z., 1997. Nomenclature of amphiboles: report of the subcommittee on amphiboles of the international mineralogical association, commission on new minerals and mineral names. Am. Mineral. 82, 1019–1037.

Li, S.G., Xiao, Y.L., Liou, D.L., 1993. Collision of the north China and Yangtse blocks and formation of coesite-bearing eclogites: timing and processes. Chem. Geol. 109, 89–111.

Liu, J.B., You, Z.D., Zhong, Z.Q., 1996. Eclogites from the middle and north of Dabie Mountains in southern Henan and northern Hubei, China. Sci. China, Ser. D 39 (3), 293–299.

Liu, J.B., Ye, K., Guo, L.J., 1998. High-pressure and ultra-high pressure eclogite in the Hong'an region, central China. Sci. Geol. Sin. 7 (4), 481–492.

Liu, X., Wei, C., Li, S., Dong, S., Liu, J., 2004. Thermobaric structure of a traverse across western Dabieshan: implications for collision tectonics between the Sino-Korean and Yangtze cratons. J. Metamorph. Geol. 22, 361–379.

Massonne, H.J., 1992. Evidence for low-temperature ultrapotassic siliceous fluids in subduction zone environments from experiments in the system K_2O–MgO–Al_2O_3–SiO_2–H_2O (KMASH). Lithos 28, 421–434.

Molina, J.F., Austrheim, H., Glodny, J., Rusin, A., 2002. The eclogites of the Marun–Keu complex, Polar Urals (Russia): fluid control on reaction kinetics and metasomatism during high *P* metamorphism. Lithos 61, 55–78.

Nakamura, D., Hirajima, T., 2000. Granulite facies overprinting of ultra-high pressure metamorphic rocks, northeastern Su-Lu region, eastern China. J. Petrol. 41 (4), 563–582.

Okay, A.I., 1993. Petrology of a diamond and coesite-bearing metamorphic terrain: Dabie Shan, China. Eur. J. Mineral. 5, 1–17.

Okay, A.I., 1995. Paragonite eclogites from Dabie Shan, China: re-equilibration during exhumation? J. Metamorph. Geol. 13, 449–460.

Perchuk, A., Philippot, P., Erdmer, P., Fialin, M., 1999. Rates of thermal equilibration at the onset of subduction deduced from diffusion modeling of eclogitic garnets, Yukon–Tanana terrane, Canada. Geology 27, 531–534.

Proyer, A., Dachs, E., McCammon, C., 2004. Pitfalls in geothermobarometry of eclogites: Fe^{3+} and changes in the mineral chemistry of omphacite at ultrahigh pressures. Contrib. Mineral. Petrol. 147, 305–318.

Rowley, D.B., Xue, F., Tucker, R.D., Peng, Z.X., Baker, J., Davis, A., 1997. Ages of ultrahigh pressure metamorphism and protolith orthogneisses from the eastern Dabieshan: U/Pb zircon geochronology. Earth Planet. Sci. Lett. 151, 191–203.

Schmidt, M.W., 1996. Experimental constraints on recycling of potassium from subducted oceanic crust. Science 272, 1927–1930.

Schmid, R., Franz, L., Oberhansli, R., Dong, S.W., 2000. High-Si phengite, mineral chemistry and *P–T* evolution of ultra-high-pressure eclogites and calc-silicates from the Dabie Shan, eastern China. Geol. J. 35, 185–207.

Schmid, R., Wilke, M., Oberhansli, R., Janssens, K., Falkenberg, G., Franz, L., Gaab, A., 2003. Micro-XANES determination of ferric iron and its application in thermobarometry. Lithos 70, 381–391.

Schulte, B., Sindern, S., 2002. K-rich fluid metasomatism at high-pressure metamorphic conditions: lawsonite decomposition in rodingitized ultramafite of the Maksyutovo Complex, southern Urals (Russia). J. Metamorph. Geol. 20, 529–541.

Scott, V.D., Love, G., Reed, S.J.B., 1995. Quantitative Electron-Probe Microanalysis. Ellis Horwood Limited, New York.

Sorensen, S.S., Grossman, J.N., Perfit, M.R., 1997. Phengite-hosted LILE enrichment in eclogite and related rocks: implications for fluid-mediated mass transfer in subduction zones and arc magma genesis. J. Petrol. 38, 3–34.

Spear, F.S., 1993. Metamorphic phase equilibria and pressure–temperature–time paths. Mineral. Soc. Am. Monogr. 573–583.

Stöckhert, B., Duyster, J., Trepmann, C., Massonne, H.J., 2001. Microdiamond daughter crystals precipitated from supercritical COH plus silicate fluids included in garnet, Erzgebirge, Germany. Geology 29, 391–394.

Tabata, H., Maruyama, S., Shi, Z., 1998. Metamorphic zoning and thermal structure of the Dabie ultrahigh-pressure–high-pressure terrane. Isl. Arc 7, 142–158.

Wang, X., Liou, J.G., Maruyama, S., 1992. Coesite-bearing eclogites from the Dabie Mountains, central China: petrogenesis, *P–T* paths, and implications for regional tectonics. J. Geol. 100, 231–250.

Wang, Q., Ishiwatari, A., Zhao, Z.Y., Hirajima, T., Hiramatsu, N., Enami, M., Zhai, M., Li, J., Cong, B., 1993. Coesite-bearing granulite retrograded from eclogite in Weihai, eastern China. Eur. J. Mineral. 5, 141–152.

Waters, D.J, Martin, H.N., 1993. Geobarometry of phengite-bearing eclogites. Terra Abstr. 5, 410–411.

Wunder, B., Melzer, S., 2003. Experimental evidence on phlogopitic mantle metasomatism induced by phengite dehydration. Eur. J. Mineral. 15, 641–647.

Yao, Y.P., Ye, K., Liu, J.B., Cong, B.L., Wang, Q.C., 2000. A transitional eclogite- to high pressure granulite-facies overprint on coesite–eclogite at Taohang in the Sulu ultrahigh-pressure terrane, eastern China. Lithos 52, 109–120.

Zhang, R.Y., Liou, J.G., 1994. Coesite-bearing eclogite in Henan Province, central China: detailed petrography, glaucophane stability and *PT* path. Eur. J. Mineral. 6, 217–233.

Zhang, R.Y., Hirajima, T., Banno, S., Cong, B.L., Liou, J.G., 1995a. Petrology of ultrahigh-pressure rocks from the southern Su-Lu region, eastern China. J. Metamorph. Geol. 13, 659–675.

Zhang, R.Y., Liou, J.G., Ernst, W.G., 1995b. Ultra-high-pressure metamorphism and decompressional *P–T* path of eclogites and country rocks from Weihai, eastern China. Isl. Arc 4, 293–309.

Zhou, G., Liu, Y.J., Eide, E.A, Liou, J.G., Ernst, W.G., 1993. High pressure low temperature metamorphism in northern Hubei Province, central China. J. Metamorph. Geol. 11, 561–574.